Journal of Applied Fluid Mechanics, Vol. 10, No. 1, pp. 307-317, 2017.
Available online at www.jafmonline.net, ISSN 1735-3572, EISSN 1735-3645.
DOI: 10.18869/acadpub.jafm.73.238.26727

Free Surface Thin Film Flow of a Sisko's Fluid over a Surface Topography

R. A. Shah[1†], P. Gaskell[2] and S. Veremieiev[2]

[1] *Basic Sciences and Islamiat Department. The University of Engineering and Technology, Peshawar, Pakistan*
[2] *School of Engineering and Computing Sciences, The University of Durham, DHI 3LE, United Kingdom*

†*Corresponding Author Email: mmrehan79@yahoo.com*

(Received June 18, 2016; accepted September 10, 2016)

ABSTRACT

The flow of a thin film down an inclined surface over topography is considered for the case of liquids with Sisko's model viscosity. For the first time lubrication theory is used to reduce the governing equations to a non-linear evolution equation for a current of a Sisko's model non-Newtonian fluid on an inclined plane under the action of gravity and the viscous stresses. This model is solved numerically using an efficient Full Approximation Storage (FAS) multigrid algorithm. Free surface results are plotted and carefully examined near the topography for different values of power-law index n_p, viscosity parameter m, the aspect ratio A and for different inclination angle θ of the plane with the horizontal. Number of complications and additional physical effects are discussed that enrich real situations. It is observed that the flows into narrow trenches develop a capillary ridge just in front of the upstream edge of a trench followed by a small trough. For relatively small width trenches, the free surface is almost everywhere flat as the dimensional width of the trench is much smaller than the capillary length scale. In this region, surface tension dominates the solution and acts so as to stretch a membrane across the trench leading to smaller height deviations. The ridge originates from the topographic forcing which works to force fluid upstream immediately prior to the trench before helping to accelerate it over. The upstream forcing slows down the fluid locally and increases the layer thickness.

Keywords: Thin films; Free surface flows; Non-newtonian films; Trench topography; Long wave Approximation; Finite elements.

1. INTRODUCTION

Mathematical modelling and numerical investigations for the free surface gravity driven thin film flow of a non-Newtonian fluid over topography have important applications due to increasing number of thin film devices that are manufactured. Industries as diverse as microelectronics, displays, optical storage or microfluidic devices all require an understanding of thin liquid film deposition. Free surface film flows occur regularly during coating and cooling processes in a wide range of industrial applications. Free-surface thin-film flows over topography have recently received considerable attention and have been the focus of several works. We briefly review some of these studies. The numerically steady solutions of the lubrication equations for flows over topographical features such as single steps (steps-down and up) and finite features (trenches and mounds) were studied by Kalliadasis *et al.* (2000). The steady state solution for the full Stokes equation for flows over topography was performed by Mazouchi and Homsy (2001). They demonstrated that the lubrication theory provides a good approximation of the flows for sufficiently small values of the capillary number. On the other hand, Gramlich *et al.* (2002) examined the possibility of levelling flows over topography by means of thermocapillary Marangoni stresses produced by localized heaters on the topographical substrate. The stability of free-surface thin-film flows over topographical features was addressed by Kalliadasis and Homsy (2001) who examined in detail the spectrum of the linearized operator of the system that governs the evolution of infinitesimal disturbances in the transverse direction. They demonstrated that flows over topographical features are asymptotically stable and they also performed an energy analysis of the associated eigen value problem to reveal the stability mechanism for such flows. The work based on the long-wave, or lubrication, approximation, arguably

the first comprehensive and detailed computational study of three-dimensional thin film flow over surface topography was performed by Gaskell *et al.* (2004). The results they obtained, using a very efficient purpose designed multigrid algorithm embodying automatic error-controlled time stepping Gaskell *et al.* (2004) to solve an implicit finite difference analogue for the film thickness and pressure, were found to be in excellent agreement with the corresponding experiments of Decré and Baret (2003), to within the experimental error reported, and to similarly capture all of the associated free-surface features mentioned above. They also quantified the expected error from the neglect of inertia, and the effect of substrate inclination angle and topography aspect ratio. In addition, they were able to establish the appropriateness of the theory underpinning the earlier linear analysis of Hayes *et al.* (2000); namely, that when inertia is negligibly small, superposition can be used to construct an appropriate free-surface response to complex topography from the knowledge of the responses to regular elementary topographies. The full Stokes equations for a gravity driven film flow over trench topography was studied by Veremieiev *et al.* (2010) and Veremieiev *et al.* (2011).

There are only few studies exist in the literature that investigate thin film flow of non-Newtonian fluids over topography. Oldroyld-B fluid over step-down topography was studied by Saprykin *et al.* (2007). Their analyses were based on the integral-boundary-layer approximation of the Navier-Stokes equations and wall/free surface boundary conditions. They studied both steady states and time-dependent flows. Also, they showed that steady states are characterized by an asymmetric capillary ridge before the entrance to the step-down and a depression immediately before the step-down much like Newtonian flows over topography. The non-Newtonian effects, gravity, and substrate topography is examined by Kim and Khayat (2002). In this theoretical study for the transient two-dimensional flow of a thin non-Newtonian film. The study is a continuation of the previous work by Khayat and Welke (2001), which focused on the influence of inertia on a Newtonian film. In their analysis they are considering the fluid to be non-Newtonian and obeying the constitutive equation of the carreau-Bird model. The flow obeying the power law model is also discussed. It is examined that the shear thinning fluid propagates downstream, while a shear thickening tends to experience a sudden built-up near the channel exist. The focus of this research work is that of obtaining detailed numerical solutions using finite element for three dimensional film flows over trench topography. The flow is considered to be obeying the constitutive equation of Sisko's model fluid. The detail analysis about applications of this model was discussed by Sisko's (1958) and Sisko's (1960). The solutions for this model may be reduced to the power law model solutions upon substituting $m=0$.

2. MATHEMATICAL MODEL

Figure 1 shows a three dimensional schematic of a time dependent gravity driven film flow, of constant thickness H_0, down a planar surface containing a well-defined topography of depth S_0 , length $L_T \ll L_S$ and width $W_T \ll W_S$, that is inclined at an angle $\theta(\neq 0)$ to the horizontal. The film flow over ($S_0<H_0$). The flow is assumed incompressible and obeying the constitutive equation of Power law fluid. The co-ordinate system is chosen at the centre of the plane in which *X*-axis is the stream wise direction, *Y*-axis is span-wise and *Z*-axis is normal to the plane. The inclined plane is referred to as *S(X,Y)* , the free surface by *S(X,Y,T)*.The film thickness, *H(X,Y,T)* , at any point in the*(X,Y)* plane is given by *H=F-S*.

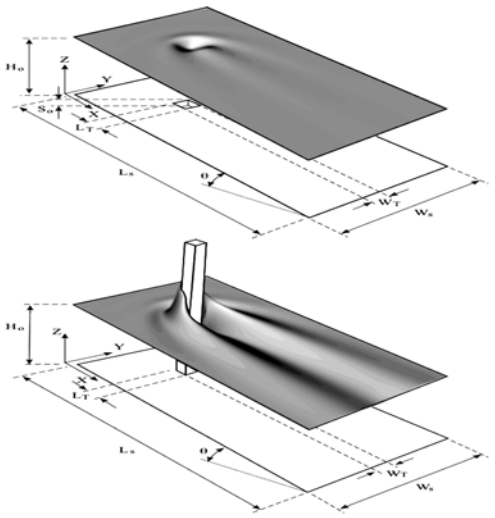

Fig. 1. Schematic diagram of thin film flow on an inclined plane over: (a) small square trench (b) and past a square occlusion.

The mass and balanced momentum equations are given as,

$$\nabla.\vec{U} = 0, \tag{1}$$

$$\rho\left(\frac{\partial \vec{U}}{\partial T} + \vec{U}.\nabla\vec{U}\right) = -\nabla\vec{\Pi} + \rho\vec{g}, \tag{2}$$

where $\vec{U} = \left(U(x,y,z,t), V(x,y,z,t), W(x,y,z,t)\right)$ is the velocity field, ρ the constant density $\vec{g} = g\left(\sin\theta, 0, -\cos\theta\right)$ is the acceleration due to gravity where g is the standard gravity constant and $\vec{\Pi}$ is the Cauchy stress tensor defined as $\vec{\Pi} = -P\vec{I} + \vec{S}$. In which $P(x,y,z)$ is the pressure, $\vec{I}$ is the identity tensor and $\vec{S}$ is the extra stress tensor. For Sisko fluid model $\vec{S}$ is defined as

$$\vec{S} = \left[m^* + \eta_0^* \left| \frac{1}{2} trac\left(\vec{A}_1^2\right) \right|^{\frac{n-1}{2}} \right] \vec{A}_1,$$

where m^* is the viscosity parameter, $\overrightarrow{A_1}$ is the kinematic tensor defined by $\overrightarrow{A_1} = \vec{L} + \vec{L}^{Transpose}$, η_0^* is the consistency index and *n* is the power law index. The consistency index is always greater than zero and is also known as viscosity coefficient. For m^*=0, the flow behavior index *n*, dictates the rheology of the fluid, i.e. *n<1* (Shear thinning), *n=1*(Newtonian) and *n>1* (Shear thickening). The variation of n from unity shows the measure of variation from Newtonian behavior. The no slip, inflow/outflow, kinematic and free surface boundary conditions are

$$U\big|_{Z=S} = 0, \tag{3}$$

$$H\big|_{X=0} = H_0, U\big|_{X=0,L_P;Y=0,W_P} = U_0 \frac{Z}{H_0} \left(2 - \frac{Z}{H_0}\right) \tag{4}$$

$$\frac{\partial F}{\partial T} + U\big|_{Z=F}\frac{\partial F}{\partial X} + V\big|_{Z=F}\frac{\partial F}{\partial Y} - W\big|_{Z=F} = 0, \tag{5}$$
$$\left(-P\vec{I} + \vec{S}\right)_{Z=F}\vec{n} = (\sigma K + P_A)\vec{n},$$

where P_A is the atmospheric pressure and taken to be zero here,

$$\vec{n} = \left(\frac{\partial F}{\partial X}\hat{l} - \frac{\partial F}{\partial Y}\hat{J} + \hat{k}\right)\left[\left(\frac{\partial F}{\partial X}\right)^2 + \left(\frac{\partial F}{\partial Y}\right)^2 + 1\right]^{-\frac{1}{2}} \tag{6}$$

is the unit normal vector pointing outward from the free surface and $K = -\nabla.\vec{n}$ is the curvature of the free surface.

The task of solving the above equations together with appropriate boundary conditions,

written in non-dimensional form using the following scalings:

$H = H_0 h$, $U = U_0 u$, $V = U_0 v$, $W = \varepsilon U_0 w$, $X = L_0 x$, $Y = L_0 y$, $Z = H_0 Z$, $F = H_0 f$, $S = H_0 s$, $T = \frac{L_0}{U_0} t$, $P = P_0 p$,

$$\eta_0^* = K\left(\frac{U_0}{H_0}\right)^n \eta_0,$$

$$m^* = \eta_0^*\left(\frac{U_0}{H_0}\right)^n m, \quad P_0 = \frac{\eta_0 U_0 L_0}{H_0}, \quad \text{where}$$

$U_0 = \frac{pgH_0^2 \sin\theta}{\eta_0}$, is the surface velocity of the undisturbed fully developed film and L_0 (with $\varepsilon = \frac{H_0}{L_0}1$) are the characteristic velocity and in-plane length scales, respectively. Here, H_0, is the characteristic film thickness of the uniform steady flow on inclined substrate. The lubrication approximation is based on the assumption that: $\varepsilon = \frac{H_0}{L_0}1$. Neglecting terms of order $\varepsilon^2 = \left(\frac{H_0}{L_0}\right)^2 1$ or higher, Eq. (2) can be written in dimensionless form as,

$$\frac{\partial p}{\partial x} - 1 = \frac{\partial}{\partial z}\left[m + \left\{\left(\frac{\partial u}{\partial u}\right)^2 + \left(\frac{\partial v}{\partial z}\right)^2\right\}^{\frac{n-2}{2}}\right]\frac{\partial u}{\partial z'} \tag{7}$$

$$\frac{\partial p}{\partial y} = \frac{\partial}{\partial z}\left[m + \left\{\left(\frac{\partial u}{\partial z}\right)^2 + \left(\frac{\partial v}{\partial z}\right)^2\right\}^{\frac{n-1}{2}}\right]\frac{\partial v}{\partial z'} \tag{8}$$

$$\frac{\partial p}{\partial z} = -\varepsilon Cot\theta, \tag{9}$$

and the boundary conditions reduces to

$$u = v = w = 0 \text{ on } z = s, \tag{10}$$

$$\frac{\partial u}{\partial z} = \frac{\partial v}{\partial z} = 0 \tag{11}$$

$$\text{and } p = -\tilde{C}a\nabla^2 f \text{ at } z = f, \tag{12}$$

where $\tilde{C}a = \frac{\varepsilon^s}{Ca}$. Integrating Eq. (9) from *z=s* to *z=f* and using the boundary conditions given in Eq. (12), we find

$$p = \varepsilon\cot\theta(f - z) - \tilde{C}a\nabla^2 f \tag{13}$$

Next, integrating Eq. (7) and (8) from *z=s* to *z=f* and imposing the boundary condition given in Eq. (11), we have

$$\frac{\partial u}{\partial z}\left[m + \left\{\left(\frac{\partial u}{\partial z}\right)^2 + \left(\frac{\partial v}{\partial z}\right)^2\right\}^{\frac{n-1}{2}}\right] = -\left(\frac{\partial p}{\partial x} - 1\right)(f - z), \tag{14}$$

$$\frac{\partial v}{\partial z}\left[m + \left\{\left(\frac{\partial u}{\partial z}\right)^2 + \left(\frac{\partial v}{\partial z}\right)^2\right\}^{\frac{n-1}{2}}\right] = -\frac{\partial p}{\partial y}(f - z), \tag{15}$$

After some algebraic manipulation of these equations and using perturbation analysis under assumption $m1$, and $\frac{\partial u}{\partial z} = \frac{\partial u_0}{\partial z} + m\frac{\partial u_1}{\partial z}$ and $\frac{\partial v}{\partial z} = \frac{\partial v_0}{\partial z} + m\frac{\partial v_1}{\partial z}$, after collecting and integrating the equations of power of order *m* it is possible to obtain

$$u = \frac{-n\left(\frac{\partial p}{\partial x} - 1\right)}{(n+1)\left(\left(\frac{\partial p}{\partial x} - 1\right)^2 + \left(\frac{\partial p}{\partial y}\right)^2\right)^{\frac{n-1}{2}}}\left[h^{\frac{n+1}{n}} - (f - z)^{\frac{n+1}{n}}\right] \tag{16}$$
$$+ \frac{m\left(\frac{\partial p}{\partial x} - 1\right)}{2\left(\left(\frac{\partial p}{\partial x} - 1\right)^2 + \left(\frac{\partial p}{\partial y}\right)^2\right)^{\frac{n-1}{n}}}\left[h^{\frac{2}{n}} - (f - z)^{\frac{2}{n}}\right],$$

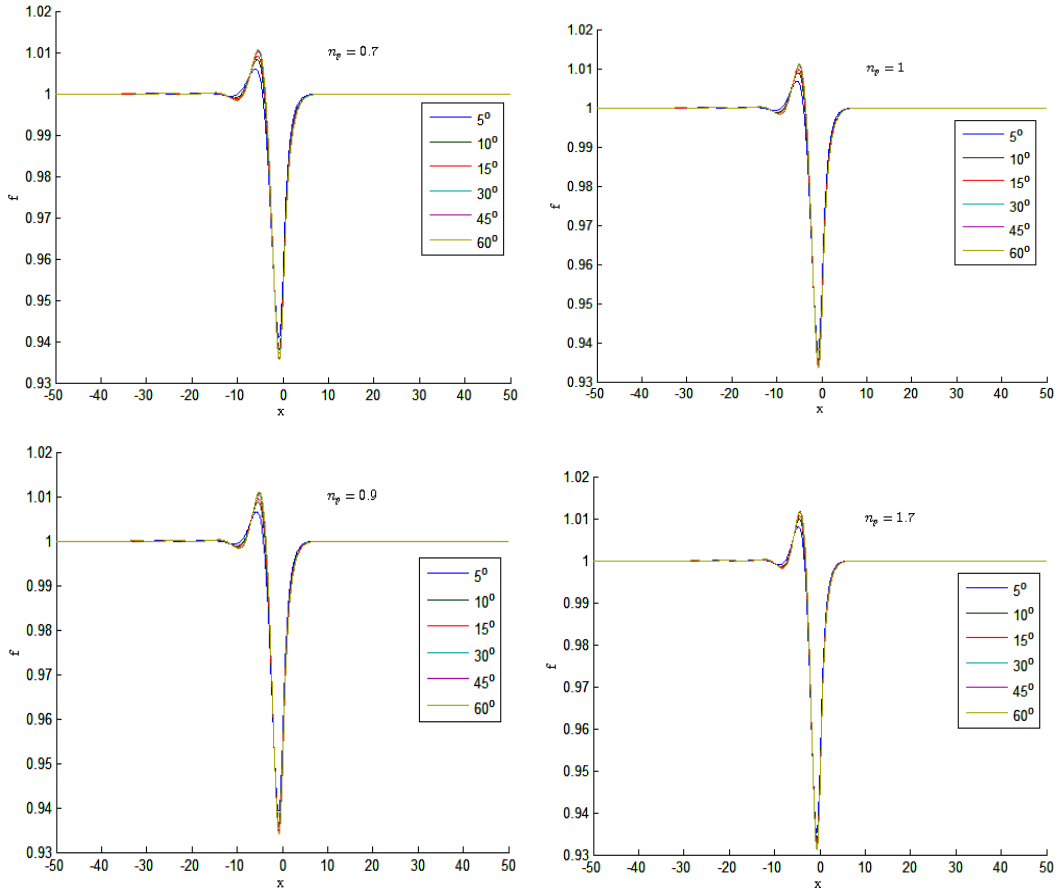

Fig. 2. Two-dimensional steady free-surface plots for flow over a localized trench topography for different values of inclination angle θ showing the effect of power law index n_p for the values $n_p = (0.7, 0.8, 0.9)$ (left) and $n_p = (1, 1.1, 1.7)$ (right) from top to bottom.

$$v = \frac{-n\dfrac{\partial p}{\partial y}}{(n+1)\left(\left(\dfrac{\partial p}{\partial x}+1\right)^2+\left(\dfrac{\partial p}{\partial y}\right)^2\right)^{\frac{n-1}{2n}}}\left[h^{\frac{n+1}{n}}-(f-z)^{\frac{n+1}{n}}\right] \quad (17)$$

$$+\frac{m\dfrac{\partial p}{\partial y}}{2\left(\left(\dfrac{\partial p}{\partial x}-1\right)^2+\left(\dfrac{\partial p}{\partial y}\right)^2\right)^{\frac{n-1}{n}}}\left[h^{\frac{2}{n}}-(f-z)^{\frac{2}{n}}\right],$$

The average velocities along streamwise $\hat{u}$ and spanwise directions $\hat{v}$ is obtain by integrating the above velocity expressions from $z=s$ to $z=f$, as

$$\hat{u} = \frac{-n\left(\dfrac{\partial p}{\partial x}-1\right)h^{\frac{n+1}{n}}}{(2n+1)\left(\left(\dfrac{\partial p}{\partial x}-1\right)^2+\left(\dfrac{\partial p}{\partial y}\right)^2\right)^{\frac{n-1}{2n}}}+ \quad (18)$$

$$\frac{m\left(\dfrac{\partial p}{\partial x}-1\right)h^{\frac{2}{n}}}{(n+2)\left(\left(\dfrac{\partial p}{\partial x}-1\right)^2+\left(\dfrac{\partial p}{\partial y}\right)^2\right)^{\frac{n-1}{n}}}$$

$$\hat{v} = \frac{-n\dfrac{\partial p}{\partial x}h^{\frac{n+1}{n}}}{(2n+1)\left(\left(\dfrac{\partial p}{\partial x}-1\right)^2+\left(\dfrac{\partial p}{\partial y}\right)^2\right)^{\frac{n-1}{2n}}}\left[h^{\frac{n+1}{n}}-(f-z)^{\frac{n+1}{n}}\right] \quad (19)$$

$$+\frac{m\dfrac{\partial p}{\partial y}h^{\frac{2}{n}}}{(n+2)\left(\left(\dfrac{\partial p}{\partial x}-1\right)^2+\left(\dfrac{\partial p}{\partial y}\right)^2\right)^{\frac{n-1}{n}}}$$

The equation of mass conservation can be written in the form

$$\frac{\partial h}{\partial t}+\frac{\partial}{\partial x}(\hat{u}h)+\frac{\partial}{\partial y}(\hat{v}h)=0 \quad (20)$$

After substituting Eq. (18) and (19) in Eq. (20) we obtain

$$\frac{\partial h}{\partial t}+\frac{\partial}{\partial x}\left(\frac{-n\left(\dfrac{\partial p}{\partial x}-1\right)h^{\frac{2n+1}{n}}}{(2n+1)\left(\left(\dfrac{\partial p}{\partial x}-1\right)^2+\left(\dfrac{\partial p}{\partial y}\right)^2\right)^{\frac{n-1}{n}}}+\frac{m\left(\dfrac{\partial p}{\partial x}-1\right)h^{\frac{2+n}{n}}}{(n+2)\left(\left(\dfrac{\partial p}{\partial x}-1\right)^2+\left(\dfrac{\partial p}{\partial y}\right)^2\right)^{\frac{n-1}{n}}}\right)$$

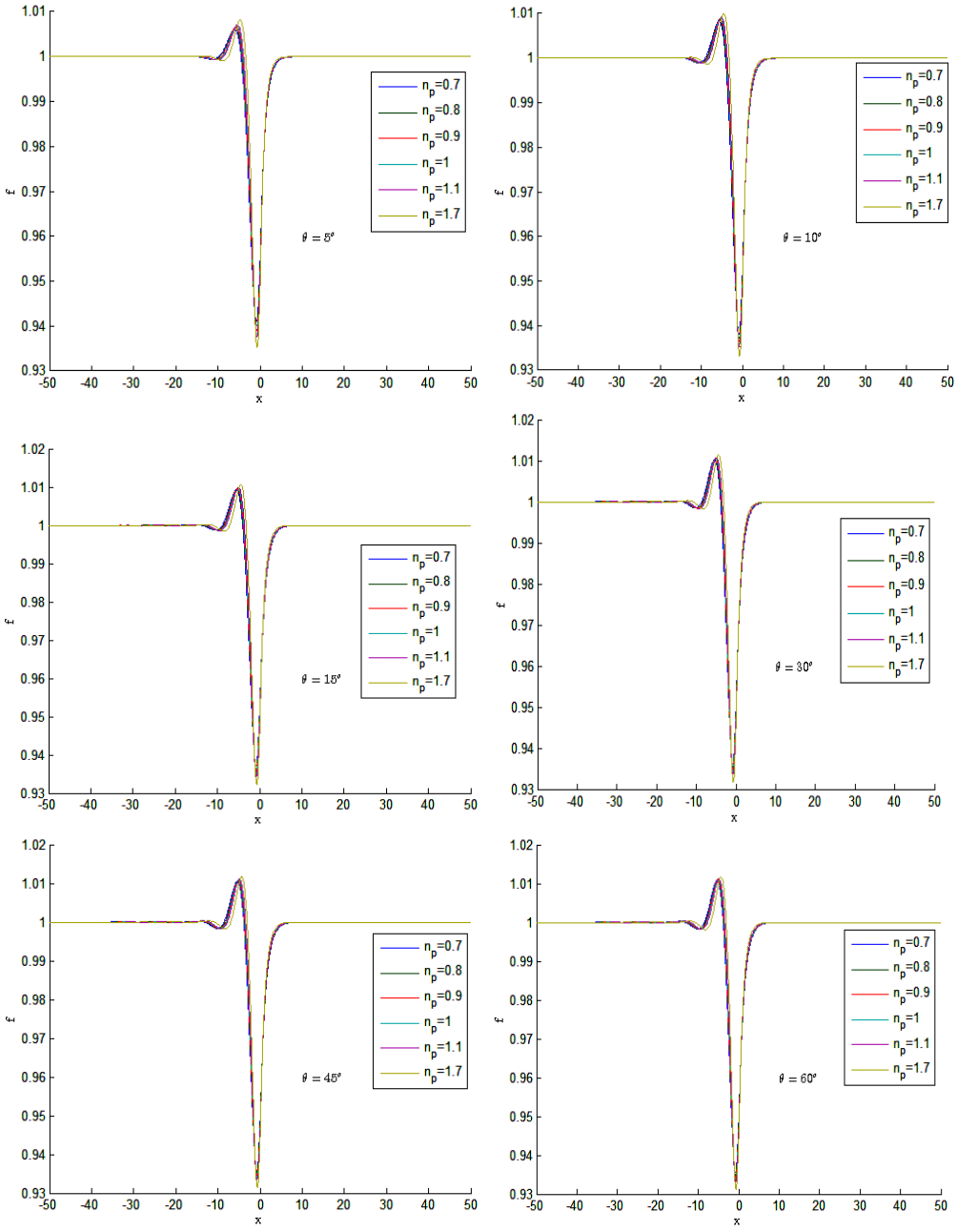

Fig. 3. Two-dimensional steady free-surface plots for flow over a localized trench topography for different values of power law index n_p showing the effect of inclination angle θ with the horizontal for the values $\theta=\left(5^0,10^0,15^0,\right)$ (left) and $\theta=\left(30^0,45^0,60^0,\right)$ (right) from top to bottom.

$$+\frac{\partial}{\partial y}\left(\frac{-n\frac{\partial p}{\partial y}h^{\frac{2n+1}{n}}}{(2n+1)\left(\left(\frac{\partial p}{\partial x}-1\right)^2+\left(\frac{\partial p}{\partial y}\right)^2\right)^{\frac{n-1}{2n}}}\left[h^{\frac{n+1}{n}}-(f-z)^{\frac{n+1}{n}}\right]+\frac{m\frac{\partial p}{\partial y}h^{\frac{2+n}{n}}}{(n+2)\left(\left(\frac{\partial p}{\partial x}-1\right)^2+\left(\frac{\partial p}{\partial y}\right)^{\frac{n-1}{n}}\right)}\right)=0 \tag{21}$$

The boundary conditions required to close the problem are that the flow is fully developed both upstream and downstream:

$$f(x=0,y)=1,\frac{\partial f}{\partial x}\Big|_{x=0}=0,\frac{\partial f}{\partial x}\Big|_{x=1}=\frac{\partial p}{\partial x}\Big|_{x=1}=0, \tag{22}$$

together with the requirement of zero flux at the boundaries in the span wise direction:

$$\frac{\partial p}{\partial y}\Big|_{y=0}=\frac{\partial p}{\partial y}\Big|_{y=1}=\frac{\partial f}{\partial y}\Big|_{y=0}=\frac{\partial f}{\partial y}\Big|_{y=1}=0, \tag{23}$$

Topography is defined via arctangent functions Stillwagon and Larson (1988) enabling the creation of simple primitive shapes. For example, a rectangular trench/peak topography of length l_t, width w_t and depth/height $|s_0|$ centred at (x_t,y_t) has the form:

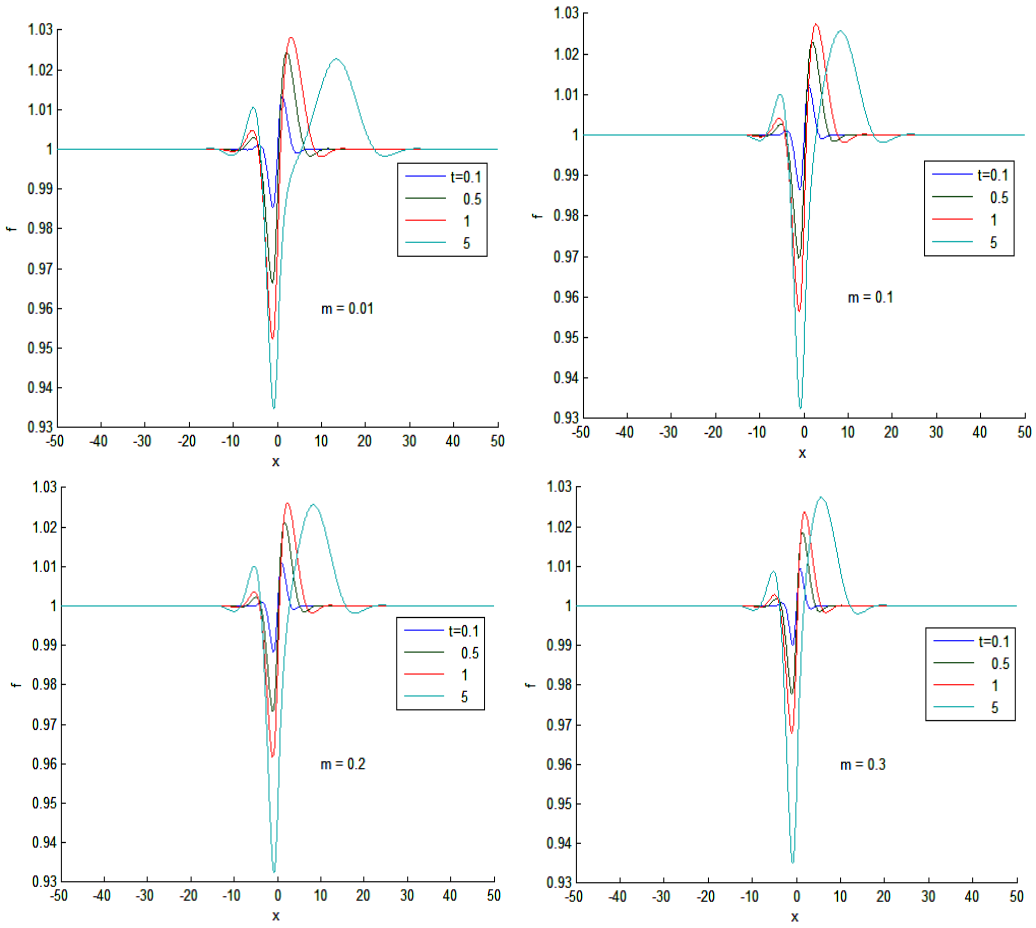

Fig. 4. Two-dimensional unsteady free-surface plots for flow over a localized trench topography for different values of time t showing the effect of viscosity parameter *m* for the values *(m=0.01,0.1)* (left) and *(m=0.2,0.3)* (right) from top to bottom.

$$S(x,y)= \frac{S_0}{b_0}\left[\tan^{-1}\left(\frac{-a_x-l_t/2}{\gamma l_t}\right)+\tan^{-1}\left(\frac{a_x-l_t/2}{\gamma l_t}\right)\right]\times\left[\tan^{-1}\left(\frac{-a_y-W_t/2}{\gamma W_t}\right)+\tan^{-1}\left(\frac{a_y-W_t/2}{\gamma W_t}\right)\right] \quad (24)$$

Where γ is adjustable parameter whose value specifies the steepness of the topography, $a_x = x_t - x$, $a_y = y_t - y$ and $b_0 = 4\tan^{-1}\left(\frac{1}{2\gamma}\right)\tan^{-1}\left(\frac{A}{2\gamma}\right)$, where $A = w_t/l_t$ is the aspect ratio of the topography.

3. THE RESULTS AND DISCUSSION

The combine effect of aspect ratio $A = w_t/l_t$, the power law index n_p and the inclination angle θ with the horizontal are discussed in Figs. 2-8. The influence of power law index n_p, on film flow over trench topography is shown in Fig. 2 for the case $\delta = 0.001$, $m = 0.01$ and for $\theta = 5^0, 10^0, 15^0, 30^0, 45^0, 60^0,$. A large asymmetric capillary ridge forms before the trench. The height of this capillary ridge is a function of the angle, θ, with the higher capillary ridges appearing for large θ. After leaving the trench, liquid takes almost flat profile. The free surface has a small depression before the capillary ridge. As n_p is increased, the height of the peak goes down, the depth of the depression starts to grow, and short-wave oscillations appear localized around the depression. Increasing n_p causes a gradual rise in and widening of the free-surface disturbance. Fig. 3 reveals the effect of n_p and θ on the stream wise free-surface profile for the flow of a thin non-Newtonian film over square trench topography. Figures 3(a-f) show the film thickness for $n_p = 0.7, 0.8, 0.9, 1, 1.1, 1.7$ and (a) $\theta = 5^0$ (b) $\theta = 10^0$ (c) $\theta = 15^0$ (d) $\theta = 30^0$ (e) $\theta = 45^0$ and (f) $\theta = 60^0$ Increasing n_p reduces the magnitude of wave length of the short wave and increases the height of the capillary ridge and the depression before the ridge. Also, It is to be noted that the bow wave migrates slightly upstream as θ decreases. Fig. 4 shows the effect of time on free surface disturbance over trench topography for

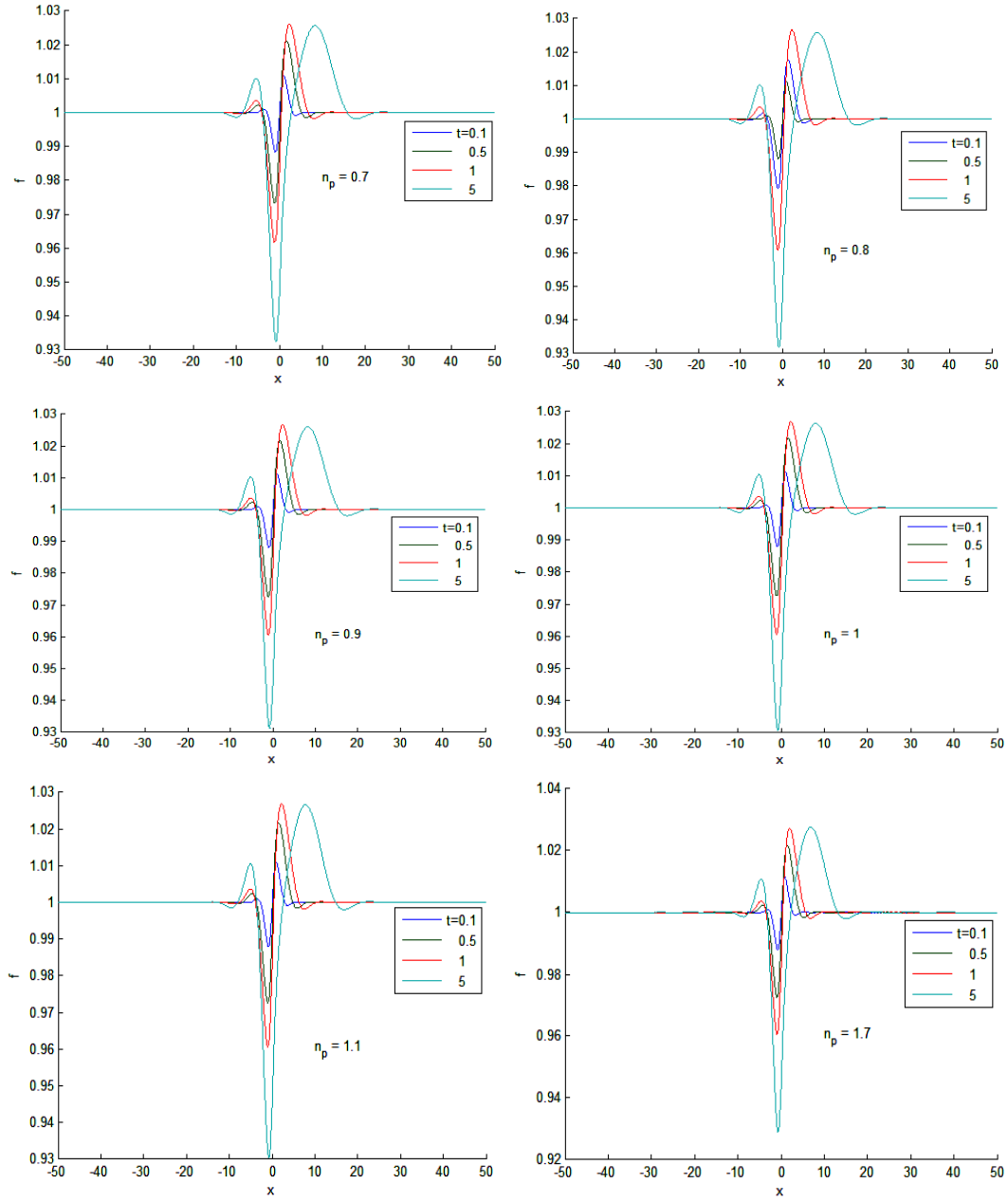

Fig. 5. Two-dimensional unsteady free-surface plots for flow over a localized trench topography for different values of time t showing the effect of power law index n_p for the values $n_p = (0.7, 0.8, 0.9)$ (left) and $n_p = (1, 0.1, 1.7)$ (right) from top to bottom.

$m = 0.01, 0.1, 0.2$ 0.3 and $n_p = 0.7$, $\theta = 30^0$, $l_t = 1, s_0 = 0.25$. It is to be noticed that the bow wave migrates upstream before interring the trench and migrates downstream after leaving the trench with the passage of time. It is interesting to note that the wave length of the wave's leaving the trench decreases as the viscosity parameter m is increases. Increasing the observation time analyse that the wave's inside the trench moves towards the bottom of trench. The free surface profile given in Fig. 5 shows the effect of time at for $n_p = 0.7, 0.8, 0.9, 1, 1.1, 1.7$, for $m = 0.2$, $\theta = 30^0$, $l_t = 1, s_0 = 0.25$. For power law model with $n_{p<1}$ predicting the flow of shear thinning liquid and for $n_{p>1}$, the phenomena is completely different and the flow offers less resistance at low shear rate. It is observed that for $n_{p>1}$ the disturbance increases near the trench and the wave's spreads more deep inside the trench. The effect of trench depth s_0 and n_p on unsteady free surface disturbance are shown in Fig. 6 (a-d) and (e-h) for different values of $n_p = 0.7, , 0.9, 1, , 1.7,$ for $m = 0.2, \theta = 30^0$ $l_t = 1, t = 1$ and $m = 0.01, 0.1,$

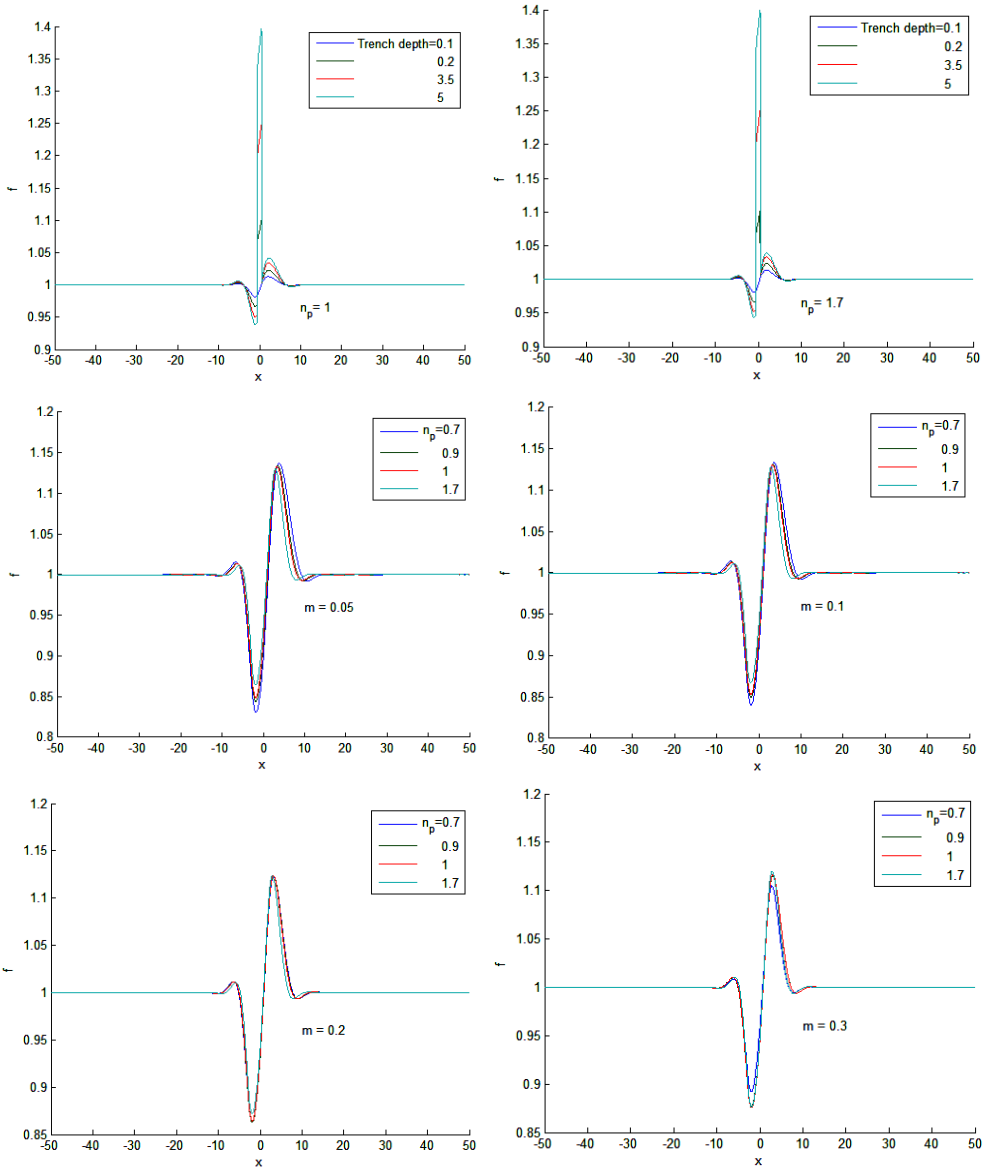

Fig. 6. Two-dimensional unsteady free-surface plots for flow over a localized trench topography at *t=1*for different values of trench depth s_0 showing the effect of power law index $n_p = 0.7, 0.9, 1, 1.7$ (left) and for different values of n_p showing the effect of viscosity parameter *m=0.01,0.1,0.2,0.3* (right) from top to bottom.

$0.2, 0.3$ for $\theta = 30^0, l_t = 5, t = 1, s_0 = 0.25$ respectively. Here, it can be seen that the capillary ridge near the trench increases with increase of trench depth. The shapes of wave's seems to be parabolic before and after the trench, while it looks to be an rectangular shape above the trench. It is to be noted that on increasing the depth of topography the height of rectangles and the parabolas increases. Fig. 7 is plotted for different values of aspect ratio *A=1,2,5,10,15,20* by keeping length of the trench fixed $l_t = 2.5, \delta = 0.001, \theta = 30^0$, and viscosity parameter *m=0.05*, to analyze the non-Newtonian fluid flow behavior over trench topography viewed from the downstream side, show that increasing trench aspect ratio *A* causes the wave to broaden and propagates towards the boundary of the plane rapidly. Increasing *A* from 1 to 20 causes the downstream flow to split into two parts lying either side of the stream wise centre-line and the height of the capillary ridge just ahead of the trench and the depth of the trough both decreasing from 1.23 to 1.17 and 0.98 to 0.84, respectively, and short-wave oscillations appear on the free surface around the capillary ridge. The shapes of waves look like parabolas for small values of aspect ratio *A=1,2* and 5, while it seems to be an open rectangular shape for the values *A=10,15* and 20. Finally, Fig. 8 show the influence of n_p on the predicted three-dimensional free-surface flow on the inclined plane $\theta = 30^0$ of dimensions $l_p = 100, \quad w_p = 100$ at $t = 0.5$ on a square localised trench with $|s_0| = 0.25, \ \delta = 0.001, \ l_t = 2.5, w_t = 2.5$ and

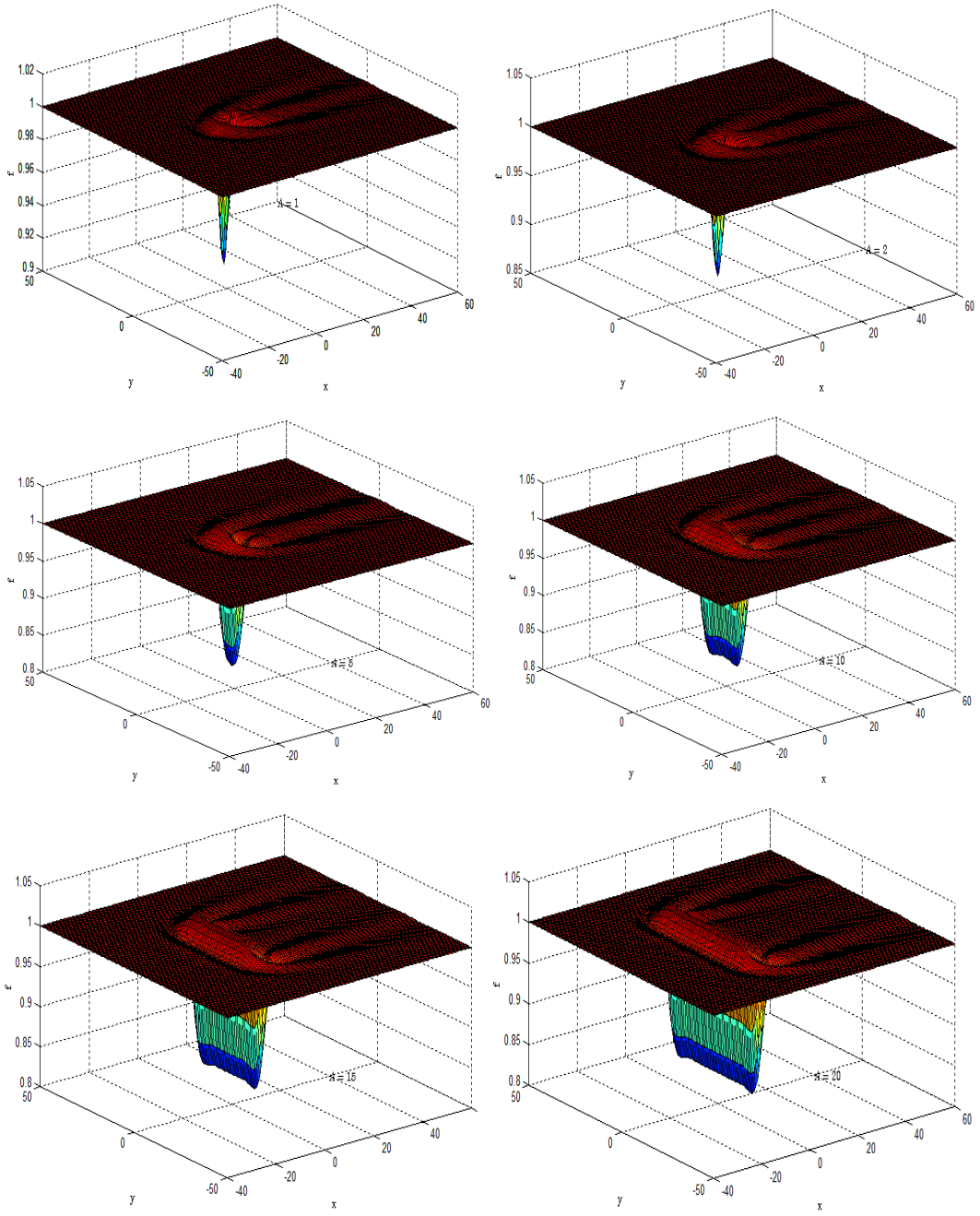

Fig. 7. Three-dimensional free-surface profiles through the centre of the topography $(x_t = -10, y_t = 0)$ for flow over a localised trench topography $(l_t = 2.5, w_t = 2.5, s_0 = 0.25)$ showing the effect of aspect ratio, $A = w_t / l_t$ for the values *(A=1,2,5)* (left) and *(A=10,15,20)* (right) from top to bottom.

the centre of the trench is located at $(x_t, y_t) = (-10, 0)$. Increasing n_p, from 0.7 to 1.7 the depth of the trough increasing from 0.84 to 0.91 and the capillary ridge of the wave increasing from 1.17 to 1.23. It can be seen from numerical data of the free surface that the maximum capillary ridge exist before the trench in the direction of flow and reducing as wave propagates towards the boundary of the surface and becomes almost flat to the initial thickness of the liquid film.

4. CONCLUSION

Three-dimensional gravity-driven flow of non-Newtonian fluid over topography has been investigated. From the context of lubrication theory and dimensional analysis, we derived a nonlinear dimensionless partial differential free surface evolution equation for the film thickness. A careful analysis of the film behavior is carried out and an extensive study has performed for a wide range of

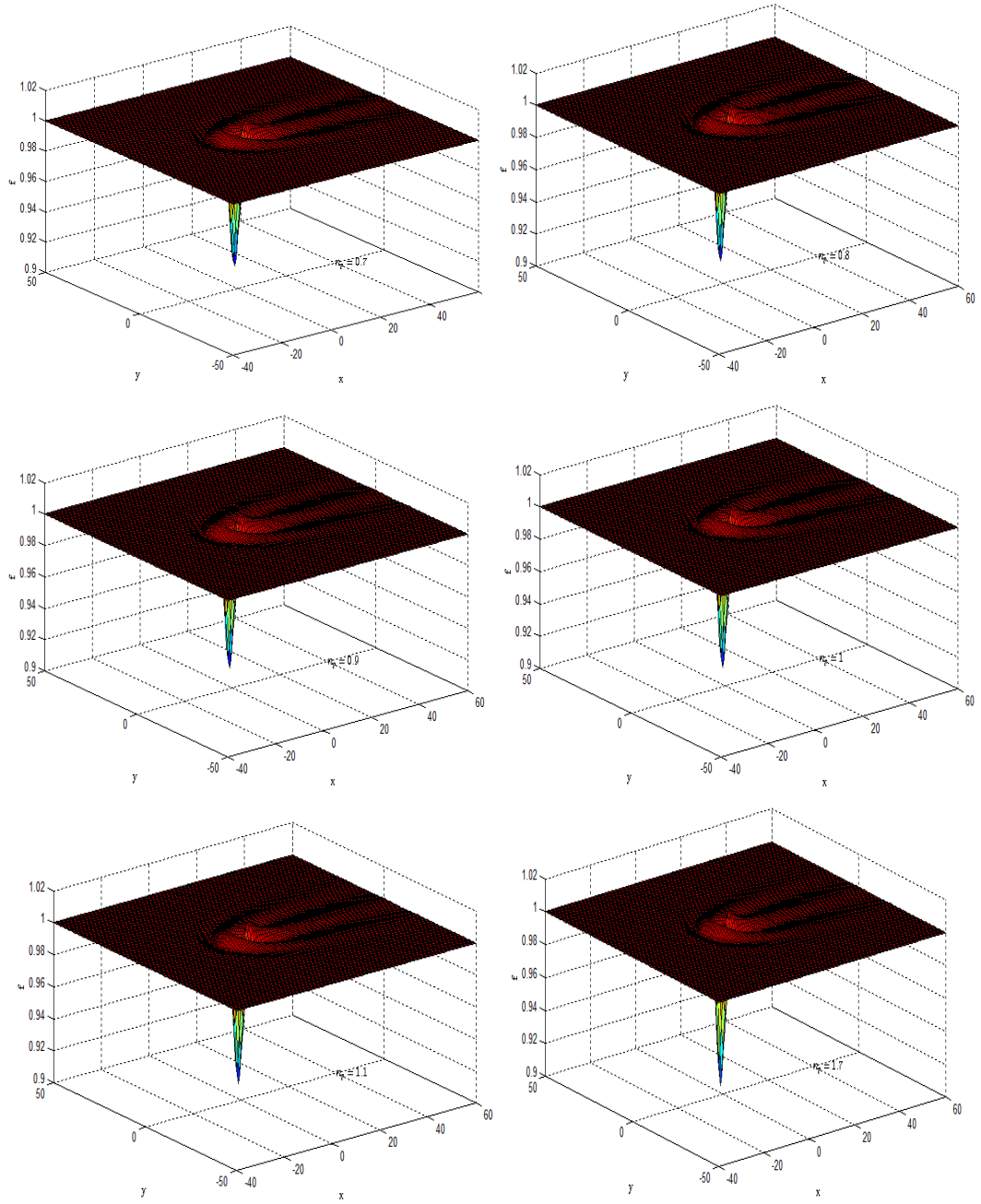

Fig. 8. Three-dimensional free-surface profiles through the center of the topography $(x_t=-10, y_t=0)$ for flow over a localised trench topography $(l_t=2.5, w_t=2.5, s_0=0.25)$ showing the effect of power law index n_p for the values $n_p=(0.7, 0.8, 0.9)$ (left) and $n_p=(1, 1.1, 1.7)$ (right) from top to bottom.

the parameters involved. The effect of power law index on flow over trenches has been examined. For the flows into narrow trenches, we have observed that the free surface develops a capillary ridge just in front of the upstream edge of a trench followed by a small trough. Also, it is observed that for relatively small width trenches, the free surface is almost everywhere flat as the dimensional width of the trench is much smaller than the capillary length scale. In this region, surface tension dominates the solution and acts so as to stretch a membrane across the trench leading to smaller height deviations. The ridge originates from the topographic forcing which works to force fluid upstream immediately prior to the trench before helping to accelerate it over. The upstream forcing slows down the fluid locally and increases the layer thickness. We note, however, that we are unable to predict accurately the flow inside the small width trench corners.

The present work has concentrated on computing unsteady solutions for gravity driven film flow over topography and there is no investigation about the stability of the capillary ridge.

ACKNOWLEDGMENTS

This research was supported by the Higher Education Commission (HEC) Pakistan under the Postdoctrate scholarship. I gratefully acknowledge financial support from the HEC, for his research studies at the Durham University, United Kingdom. I also, thankful to Durham University administration that they provide me the facility to perform this research because without the University support this research was not possible for me.

REFERENCES

Decré, M. M. J. and J. C. Baret (2003). Gravity-driven flows of viscous liquids over two-dimensional topographies. *J. Fluid Mech.* 487, 147-166.

Gaskell, P. H., P. K. Jimack, M. Sellier and H. M. Thompson (2004). Efficient and accurate time adaptive multigrid simulation of droplet spreading. *Int. J. Num. Meth. Fluids* 45, 1161-1186.

Gaskell, P. H., P. K. Jimack, M. Sellier, H. M. Thompson and M. C. T. Wilson (2004). Gravity-driven flow of continuous thin liquid films on non-porous subsrates with topography. *J. Fluid Mech.* 509, 253-280.

Gramlich, C. M., S. Kalliadasis, G. M. Homsy and C. Messer (2002). Optimal levelling of flowover one-dimensional topography by Marangoni stresses. *Phys. Fluids* 14, 1841-1850.

Hayes, M., S. B. G. O'Brien and J. H. Lammers (2000). Green's function for steady flow over a small two-dimensional topography. *Phys. Fluids* 12, 2845-2858.

Kalliadasis, S. and G. M. Homsy (2001). Stability of free-surface thin-film flows over topography *J. Fluid Mech.* 448, 387-410.

Kalliadasis, S., C. Bielarz and G. M. Homsy (2000). Steady free-surface thin film flows over topography. *Phys. Fluids* 12, 1889-1898.

Khayat, R. E. and S. Welke (2001). Influence of inertia, gravity and substrate topography on the two-dimensional transient coating flow of a thin Newtonian fluid film. *Phys. Fluids* 13, 355-368.

Kim, K. M. and R. E. Khayat (2002). Transient coating flow of a thin non-Newtonian fluid film. *Phys. Fluids* 14, 2202-2215.

Mazouchi, A. and G. M. Homsy (2001). Free surface Stokes flow over topography. *Phys. Fluids* 13, 2751-2761.

Saprykini, S., R. J. Koopmans and S. Kalliadasis (2007). Free-surface thin-film flows over topography: influence of inertia and viscoelasticity. *J. Fluid Mech.* 578, 271-293.

Sisko, A. W. (1958). The flow of lubricating greases. *Ind. Engg. Chem.* 50, 1789-1792.

Sisko, A. W. (1960). Capillary viscometer for non-Newtonian liquids. *Colloid Sci*. 15, 89-96.

Veremieiev, S., H. M. Thompson, Y. C. Lee and P. H. Gaskell (2010). Inertial thin film flow on planar surfaces featuring topography. *Comput. Fluids* 39, 431–450.

Veremieiev, S., P. H Gaskell, Y. C Lee and H. M. Thompson (2011). Predicting three-dimensional inertial thin film flow over micro-scale topography. *Computational Fluid Dynamics-Proceedings of the 6th International Conference on Computational Fluid Dynamics, ICCFD 2010,* 833-838.